Appl. Phys. B (2014) 115:45–54
DOI 10.1007/s00340-013-5571-6

Applied Physics B
Lasers and Optics

A high-harmonic generation source for seeding a free-electron laser at 38 nm

Theophilos Maltezopoulos · Manuel Mittenzwey · Armin Azima · Jörn Bödewadt · Hatem Dachraoui · Marie Rehders · Christoph Lechner · Michael Schulz · Marek Wieland · Tim Laarmann · Jörg Roßbach · Markus Drescher

Received: 5 March 2013 / Accepted: 28 June 2013 / Published online: 17 August 2013

Abstract Direct seeding with a high-harmonic generation (HHG) source can improve the spectral, temporal, and coherence properties of a free-electron laser (FEL) and shall reduce intensity and arrival-time fluctuations. In the seeding experiment sFLASH at the extreme ultraviolet FEL in Hamburg FLASH, which operates in the self-amplified spontaneous emission mode (SASE), the 21st harmonic of an 800 nm laser is refocused into a dedicated seeding undulator. For seeding, the external light field has to overcome the noise level of SASE; therefore, an efficient coupling between seed pulse and electron bunch is mandatory. Thus, an HHG beam with a proper divergence, width, beam quality, Rayleigh length, pointing stability, single-shot pulse energy, and stability in the 21st harmonic is needed. Here, we present the setup of the HHG source that seeds sFLASH at 38.1 nm, the optimization procedures, and the necessary diagnostics.

T. Maltezopoulos (✉) · M. Mittenzwey · A. Azima · J. Bödewadt · M. Rehders · C. Lechner · M. Schulz · M. Wieland · J. Roßbach · M. Drescher
Department of Physics, University of Hamburg, Luruper Chaussee 149, 22761 Hamburg, Germany
e-mail: theophilos.maltezopoulos@desy.de

T. Maltezopoulos · M. Rehders · J. Roßbach · M. Drescher
Center for Free-Electron-Laser-Science (CFEL), Luruper Chaussee 149, 22761 Hamburg, Germany

H. Dachraoui · M. Schulz · T. Laarmann
Deutsches Elektronen-Synchrotron (DESY), Notkestrasse 85, 22607 Hamburg, Germany

T. Laarmann · M. Drescher
The Hamburg Centre for Ultrafast Imaging (CUI), Luruper Chaussee 149, 22761 Hamburg, Germany

1 Introduction

The free-electron laser in Hamburg (FLASH), which operates in the self-amplified spontaneous emission mode (SASE) [1], is currently the most intense femtosecond (fs) SASE light source in the extreme ultraviolet (EUV) wavelength regime [2–4]. However, the statistical nature of the SASE process leads to intensity and spectral fluctuations in the EUV pulses and to uncorrelated laser modes, which reduce the degree of longitudinal coherence. Moreover, the electron acceleration process introduces arrival-time fluctuations in the electron bunch at the undulator entrance, which leads to a temporal jitter of the intense EUV pulses at the experimental end station with respect to a synchronized external pump–probe laser. The spectral and arrival-time fluctuations limit the energy and temporal resolution of corresponding pump–probe experiments, respectively. As a work-around, several diagnostic tools have been developed at FLASH in order to measure pulse by pulse the energy [5], temporal profile [6], and arrival time [7] of the SASE EUV pulses. With this pulse tagging approach, one can categorize and sort the measured data, thereby increasing, for instance, the temporal resolution for dynamic studies [8–11].

Another way to increase the temporal resolution and the longitudinal coherence is pursued in a seeding project called sFLASH [12–14]: The EUV seed pulses from a high-harmonic generation (HHG) source are overlapped in space and time with the electron bunches in dedicated variable-gap undulators. An HHG light source provides temporally and spatially coherent radiation in the EUV and soft X-ray region, and its well-defined phase properties even allow the formation of single attosecond pulses or pulse trains [15, 16]. Several HHG sources for seeding a free-electron laser (FEL) are discussed in the literature

[17–19]. First seeding of an FEL using an HHG source has been demonstrated at the SPring-8 compact SASE source at 160 nm [20]. Later, direct seeding at 61.2 nm has been shown at the same facility [21]. At the FEL of the SPARC facility, direct seeding at 266 nm and up-conversion with an FEL cascade to 133 nm have been demonstrated [22]. In a first stage of the sFLASH experiment, direct seeding at the 21st harmonic of an 800 nm drive-laser (38.1 nm) has been demonstrated [23, 24]. By this means, we use an FEL as single-pass amplifier for HHG radiation. A fraction of the 800 nm pulse energy and the amplified HHG radiation can be used for pump–probe experiments, where both pulses are intrinsically synchronized. Thus, with a seeded FEL, the arrival-time fluctuations in the EUV pulse relative to the HHG drive-laser pulse are expected to be strongly reduced and the stable HHG spectrum with a high degree of longitudinal coherence should be imprinted into the seeded radiation.

At sFLASH, the HHG source and the center of the first seeding undulator module are 28 m apart. Owing to radiation protection and geometry constraints, this requires one spherical multilayer and four grazing-incidence mirrors leading to a measured beamline transmission of 5 % [25]. The spherical mirror allows a magnifying 1:1.2 refocussing of the 21st harmonic into the first seeding undulator module.

Note that fluence and not simply the energy of the 21st harmonic in the first sFLASH undulator is the crucial parameter for successful seeding. Since the image into the undulator is fixed to a 1:1.2 magnification, an EUV source with a width similar to the electron bunch $w_{\mathrm{e,und}} =$ 200–400 μm [26] (widths are defined as $w = 2\sigma$) is required with sufficient intensity to overcome the noise level of the SASE process. Correspondingly, the source size is fixed, and any scaling of the HHG pulse energy by looser near-infrared (NIR) focusing is futile for the seeding purpose because the additional energy cannot be coupled into the electron bunch. In order to estimate the equivalent shot noise energy, which competes with the seed pulse and generates the SASE background, we calculate the equivalent input field generated by the electron beam following a procedure explained in [25, 27]. Taking into account the electron beam size, the equivalent FEL amplifier input pulse energy due to shot noise in the time window of the HHG pulse is about 20 pJ. Similar results are obtained following the approach of [28], where the shot noise power is directly estimated from the electron beam parameters. Taking the beamline transmission of 5 % and a coupling overlap efficiency of 25 % into account, this leads to a required minimum pulse energy of the 21st harmonic source of considerably more than 1.6 nJ. The 12.4 m long beamline from the HHG source to the focussing mirror sets an upper limit for the half-angle divergence of 1 mrad. Additionally, the source has to be stable in pulse energy and position over a total beamline length of 28 m and over several hours or days of operation. This sets high requirements to the NIR drive-laser system. Moreover, the laser system has to be synchronized to the FLASH facility on a few tens of fs level [29].

Here, we present the HHG source and the seed injection system which meets these requirements and which allowed for the first time to directly seed an FEL at 38.1 nm [23, 24]. In addition to the setup, all necessary diagnostics for tailoring and analyzing the HHG source will be presented. A realistic evaluation of the 21st harmonic pulse energy is mandatory for seeding and includes careful measurements of the absolute transmission of the thin Al foils used as laser-blocking filters.

2 Experimental setup

The experimental setup of the sFLASH HHG source and the seed beam transport is depicted in Fig. 1. The following subsections describe the laser system, HHG source, diagnostic tools, optimization parameters, and the refocussing of the HHG radiation into the sFLASH undulator.

2.1 Laser system

We use a commercial laser system based on chirped-pulse amplification, which consists of an Ti:sapphire oscillator (Compact Oscillator, Femtosource) and a stretcher with amplifier (Hidra, Coherent). The oscillator operates at 108 MHz and is electronically synchronized to the 1.3 GHz master clock of the FLASH facility [29]. The central wavelength is 800 nm with a bandwidth of 60 nm full width at half-maximum (FWHM) and a pulse energy around 4 nJ. The combined regenerative and multipass amplifier is pumped by a flash-lamp-driven Nd:YAG laser (Spitlight 600, InnoLas) operating at 10 Hz. After stretching to 150 ps FWHM, the pulses are amplified up to 50 mJ (7 mm FWHM beam diameter) with a pulse-by-pulse energy stability of down to 2 % rms over several hours.

2.2 HHG setup

Due to space restrictions of the facility, the HHG source is located below the laboratory floor level in a pit (Fig. 1), which is connected to the FLASH accelerator tunnel. This location limits the HHG source and diagnostics in several points, which will be discussed later in the text. Further details about the experimental environment and the sFLASH HHG source can be found in [30]. In order to avoid nonlinear dispersion effects in air, the uncompressed

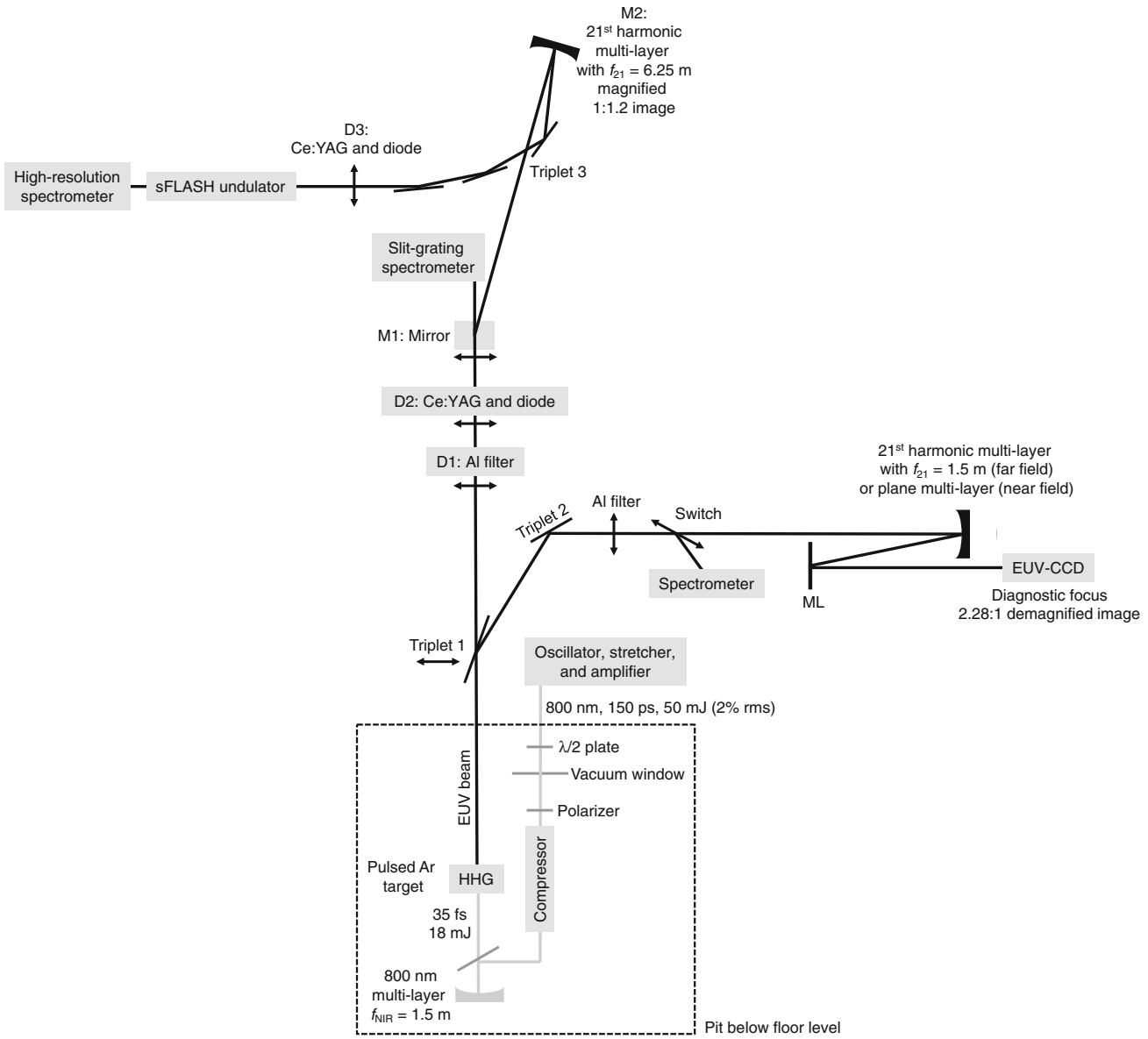

Fig. 1 Experimental setup of the HHG seeding source at FLASH: The HHG target chamber is located under the floor in a pit and is connected to the FLASH accelerator vacuum system. The NIR compressor and the focussing mirror are placed inside the target vacuum chamber. The HHG pulses can be guided to a diagnostic unit on the laser table (over 2 triplet mirrors) or to the FLASH tunnel for seeding. The diagnostic unit in the laser laboratory includes a spectrometer, a far-field, and a near-field monitor. The diagnostic unit in the tunnel includes a diode, a YAG screen, and a slit-grating spectrometer. In the FLASH accelerator tunnel, the HHG pulses are focussed and guided to the sFLASH undulators. A high-resolution soft X-ray spectrometer behind the undulators analyzes the HHG and seeded FEL radiation

laser pulses are transported into the pit. After passing a half-wave plate and a motorized iris, they are coupled through a thin vacuum window into the HHG target chamber. In vacuum, they pass a polarizer and are compressed with a grating compressor to 35 fs FWHM and loosely focused with an $f_{\mathrm{NIR}} = 1.5$ m spherical mirror into a pulsed argon gas medium. The central wavelength is still at 800 nm, but the bandwidth is reduced to 30 nm FWHM due to gain narrowing. The half-wave plate and the polarizer are inserted in order to remove possible circular polarization contributions. The polarization plane of the NIR and therefore of the HHG radiation is oriented parallel to the floor. The laser compressor is aligned by measuring the NIR pulse duration with a frequency-resolved optical gating (GRENOUILLE, Swamp Optics). In order to prevent astigmatism, the spherical mirror is irradiated under almost normal incidence. Due to losses in the compressor, half-wave plate, and polarizer, 18 mJ of the initial 50 mJ is

available at the gas target. A 50 mm long gas-cell with an inner diameter of 2 mm that is mounted directly on a pulsed argon gas nozzle (Series 9 pulse valve, Parker) is used as a target. The optimal backing pressure is around 2 bar, and the opening time is set to 400 μs. The gas target is mounted on a x, y, and z translation stage and can be scanned ±150 mm through the NIR focus in z direction. The optimal gas target position is found empirically around 50 mm in front of the laser focus. During operation, the vacuum pressure in the HHG source chamber rises to about 2×10^{-4} mbar. Two differential pumping stages are used in order to reduce the pressure to $<9 \times 10^{-7}$ mbar in the last chamber, which represents an interface to the FLASH accelerator ultra-high vacuum. In the first of the two chambers, an electron multiplier (R2362, Hamamatsu) serves as an ion detector for online monitoring the yield of individual EUV pulses. Its signal integrates over all ionizing harmonic orders of the source, and it is noninvasive and delivers a single-shot signal proportional to the HHG energy.

2.3 HHG diagnostics setup

From the source, the HHG radiation can be guided to the FLASH tunnel for seeding and, alternatively, to several diagnostic sections. The first diagnostic unit is located in the same laser laboratory. Two groups of three mirrors (triplets 1 and 2) reflect the EUV light from the pit up to the laser table. The three B_4C-coated 15° grazing-incidence mirrors in each triplet provide a significant better total reflectivity than a single 45° mirror. Between two stray-light apertures, we include several Al filters (Lebow) for blocking the fundamental laser beam. A motorized mirror reflects the harmonic radiation to a spectrometer, or, if removed, it allows the light to pass to a diagnostic-focus section. Here, the 21st harmonic is focused under near-normal incidence with a Sc/Si-coated spherical multilayer mirror with $f_{21} = 1.5$ m focal length onto a calibrated vacuum EUV-CCD (PIXIS-XO, Princeton Instruments), which is mounted on a linear stage for scanning through the focus (400 mm scan range). This diagnostic-focus is a 2.28:1 demagnified image of the source while the imaging into the sFLASH undulator employs a 1:1.2 magnification. The spherical mirror is located on a motorized switch which also carries a plane multilayer mirror for near-field measurements. Thus, near- and far-field of the 21st harmonic can be imaged onto the EUV-CCD.

The first mirror system (triplet 1) can be moved out of the light path in order to allow the seed beam to pass into the FLASH tunnel. In this branch of the beamline, there are three motorized stages. The first one (D1) carries Al filters to block the NIR laser. The second one (D2) carries a diode [AXUV300C/AI, 300 nm Al coating, International Radiation Detectors (IRD)] for energy measurements and a cerium-doped YAG (Ce:YAG) screen with camera for monitoring the position of the harmonic radiation. A mirror on the third stage (M1) reflects the light to the FLASH accelerator tunnel, or, if removed, let it pass to a slit-grating spectrometer. Two free-standing slit-gratings are available, both fabricated on a thin Si_3N_4 membrane with 90 μm slit width and 1 mm slit height (ZonePlates.com). The first slit-grating has 2,500 lines/mm with a resolving power of $\lambda/\Delta\lambda = 130$ at $\lambda = 38.1$ nm (calculated according to [31]) and resolves harmonic orders ≥19. The second one has 1,250 lines/mm and is suited for the detection down to the 9th harmonic (88.9 nm). It covers the full HHG spectrum with $\lambda/\Delta\lambda = 66$ for the 21st harmonic order. The detector is a microchannel plate (MCP) with phosphor screen which is imaged onto a CCD camera outside the vacuum.

2.4 HHG optimization

At the current stage of the sFLASH experiment, the 21st harmonic is used for seeding. The equipment of the HHG source together with the diagnostic tools described above is used to optimize this harmonic order. Efficient seeding requires a combination of defined divergence, beam quality M^2, Rayleigh length z_R, and beam width w ($w = 2\sigma$). Also, the stability of beam position and angle, as well as of the energy of the 21st harmonic order E_{21} is important for reliable seeding of the electron bunch. The near-field monitor is used for the divergence measurement, while the diagnostic-focus scan delivers M^2, z_R, w, and the pointing stability. With the calibrated EUV photodiode, one can deduce E_{21} and its stability. Pulse energy and stability can also be extracted from the data of the calibrated EUV-CCD, which is operated behind two multilayer mirrors to selectively image only the 21st harmonic. For optimizing the HHG source, the signal of the EUV-CCD is observed, and the iris diameter, compressor position, gas target position relative to the NIR focus, and timing of the gas nozzle relative to the NIR laser pulses are tuned to maximum energy in the 21st harmonic. All parameters are tuned iteratively until the highest pulse energy is obtained. A subsequent characterization of the focus in the diagnostic section checks whether M^2, z_R, w, and the pointing stability are within the tolerable boundaries and the near-field monitor is used to verify a divergence below 1 mrad.

The iris diameter is varied in order to optimize the NIR pulse energy and focus diameter at the HHG target. By increasing the iris diameter, the HHG output increases until plasma formation starts to reduce the HHG efficiency again [15]. The timing of the gas nozzle relative to the NIR laser adjusts the Ar pressure at the target. Again, with increasing

gas pressure, the HHG yield increases until a maximum is reached. At higher pressures, absorption or phase mismatch reduces the HHG output [16].

As mentioned above, sufficient seed intensity, i.e., fluence per pulse duration, is a crucial parameter for reliable seeding. The far-field diagnostic with the EUV-CCD measures the energy of the 21st harmonic (E_{21}) and the diagnostic-focus width (w_{21}). Thus, it can be used to optimize for maximum energy E_{21} or for maximum fluence E_{21}/w_{21}^2. The realized settings yield the same HHG source parameters for energy and fluence optimization; therefore, maximum energy corresponds to maximum fluence.

2.5 HHG focussing into the first sFLASH undulator module

From the HHG source, the EUV seed radiation is guided to the first sFLASH undulator module with one Sc/Si-coated spherical multilayer and four B_4C-coated plane grazing-incidence mirrors (see Fig. 1). The first grazing-incidence mirror M1 deflects the beam vertically from the pit level to the FLASH accelerator beam height. The spherical mirror M2 with $f = 6.25$ m (nominal) selects the 21st harmonic and forms a magnified 1:1.2 image of the source, which is directed into the first undulator module with the three plane mirrors (triplet 3 in Fig. 1). A Ce:YAG screen and a diode can be moved into the beam path in order to measure the seed beam spatial profile and energy, respectively. The 21st harmonic is the shortest wavelength of the argon harmonic spectrum which still has a tolerable transmission through the beamline of 5 %. Shorter wavelengths are subject to much lower transmissions and further reduce the available seed power in the undulator. Further details and the design of the injection beamline can be found in [25]. Behind the four seeding undulator modules, a spectrometer with $\lambda/\Delta\lambda \approx 700$ and a range between 1.7 and 39.2 nm (model 248/310 UHV, 1 m grazing incidence, McPherson) analyzes the spectral details of the HHG or seeded FEL radiation.

3 Seed source characterization

This section starts with the NIR laser characterization including a characterization of the NIR focus and pulse-duration measurements. Harmonic spectra will be presented together with a diagnostic-focus scan of the 21st harmonic. The stability of the source and the average single-shot pulse energy will be evaluated. Additionally, the transmission of the NIR-suppressing Al filters has been measured, which is important for the deduction of absolute pulse energies from EUV-CCD and diode data. Finally, energy and spatial profile of the 21st harmonic in front of the first seeding undulator will be discussed.

3.1 Laser diagnostics

For HHG, the 800 nm laser has to be focussed in space and compressed in time. For aligning the in-vacuum compressor, the target chamber was vented and diagnostic tools were temporarily installed: A GRENOUILLE autocorrelator was used to monitor the pulse duration, and the gas nozzle was exchanged with a CCD camera in order to measure the focus shape. Successively, the compressor was aligned to best focus shape and temporal compression. After optimization, the pulse duration was 35 fs FWHM. The HHG pulse duration cannot be measured with the current setup but is expected to be significantly shorter than the one of the fundamental laser [32, 33]. The focus quality was measured with a through-focus scan shown in Fig. 2. For the focus scan with $f_{\mathrm{NIR}} = 1.5$ m, the iris was fully opened. At each scan position z, the beam waist was imaged with the CCD camera and the width w was obtained by using the second-moment evaluation [34, 35] for the x (horizontal) and y (vertical) directions. The data were fitted to:

$$w(z) = w_0 \cdot \sqrt{1 + \left(\frac{z-b}{z_{\mathrm{R}}}\right)^2} \tag{1}$$

and

$$M^2 = \frac{\pi w_0^2}{z_{\mathrm{R}}\lambda} \tag{2}$$

and M^2, w_0, and z_{R} in x and y were extracted. The parameter b gives the focus position in x and y, and thus, it is a measure for the astigmatism. The fit parameters are $w_{0,\mathrm{NIR},x} = (120 \pm 2)$ µm, $w_{0,\mathrm{NIR},y} = (109 \pm 1)$ µm, $z_{R,\mathrm{NIR},x} = (38 \pm 1)$ mm, $z_{R,\mathrm{NIR},y} = (48 \pm 2)$ mm, $M^2_{\mathrm{NIR},x}$

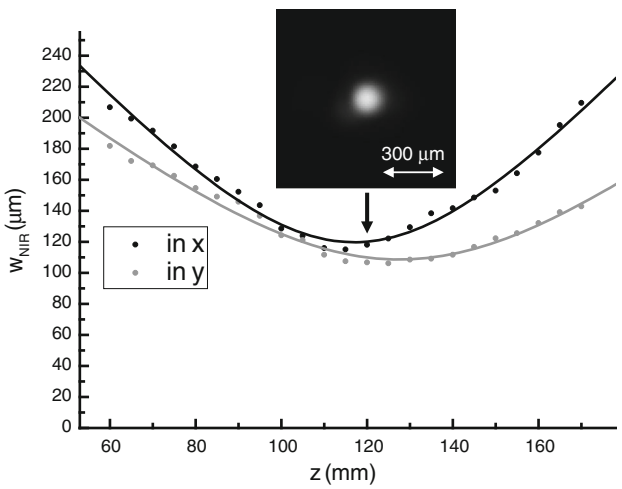

Fig. 2 NIR focus scan at the gas target ($f_{\mathrm{NIR}} = 1.5$ m): An astigmatism of 10 mm is observed. Measured widths in horizontal x and vertical y direction (*points*) and fitted curves (*lines*). *Inset* picture of NIR focus at the indicated position

$= 1.49 \pm 0.06$, and $M^2_{\mathrm{NIR},y} = 0.97 \pm 0.04$ with a slight astigmatism of $b_{\mathrm{NIR},y} - b_{\mathrm{NIR},x} = 10$ mm. Note that data points further apart from the NIR focus, which are needed for a proper second-moment evaluation, could not be taken due to space restrictions. We assume that this is the reason why $M^2_{NIR,y}$ is slightly below 1. With an NIR energy of 18 mJ, a pulse duration of 35 fs FWHM, and an average width of 115 μm, the maximum achievable intensity is calculated to be $1.2 \times 10^{15}\,\mathrm{W/cm^2}$.

3.2 HHG diagnostics

A spectrum of the optimized HHG source is shown in Fig. 3a. It is measured with the slit-grating spectrometer in the FLASH tunnel (2,500 lines/mm grating). The HHG cutoff is found at the 31st harmonic. A Gaussian fit of the 21st harmonic spectrum has a width of 0.69 nm FWHM. The slit-grating spectrometer is designed to cover the full HHG spectrum and is not optimized for resolution. At 38.1 nm the resolution is limited to 0.29 nm FWHM, i.e., $\lambda/\Delta\lambda = 130$. Additionally, the MCP, fluorescence screen, and image of the screen can broaden the lines. Figure 3b shows a high-resolution spectrum of the 21st harmonic obtained with the spectrometer behind the undulators. The resolution $\lambda/\Delta\lambda \approx 700$ now yields a linewidth of $\Delta\lambda =$ 0.24 nm FWHM. Assuming a Gaussian profile with a time-bandwidth product of 0.441 sets a lower bound of the seed pulse duration of 9 fs FWHM:

$$\Delta t = 0.441 \frac{\lambda^2}{c \cdot \Delta\lambda} = 9\,\mathrm{fs} \tag{3}$$

A diagnostic-focus scan of the 21st harmonic can be carried out with the far-field branch of the diagnostic section. A typical scan is shown in Fig. 4. The same analysis as described for the case of the NIR focus scan now yields an astigmatism of $b_{21,y} - b_{21,x} = 66$ mm. As in the NIR case, the x-focus is located in front of the y-focus. The other fit parameters are $w_{0,21,x} = (71 \pm 10)$ μm, $w_{0,21,y} =$ (30 ± 8) μm, $z_{R,21,x} = (44 \pm 7)$ mm, $z_{R,21,y} = (17 \pm 5)$ mm, $M^2_{21,x} = 9.5 \pm 3.1$, and $M^2_{21,y} = 4.4 \pm 2.7$. The distance between the gas target and the focussing mirror is about 4.9 m, while the distance between the focus-mirror and the position in between both astigmatic foci is about 2.15 m. These values are close to the ones calculated with geometrical optics, which we attribute to the fact that the distance from the HHG source to the diagnostic section is much larger than the Rayleigh length. The astigmatism of 66 mm cannot be explained by the off-axis 3° incidence reflection from the spherical mirror, which would result in sagittal and meridional foci at 1.502 and 1.498 m, respectively. Using geometrical optics, this would lead to an astigmatism of 8 mm in worst case. We assume that the abberations of the EUV wavefront are induced by the six triplet and two multilayer

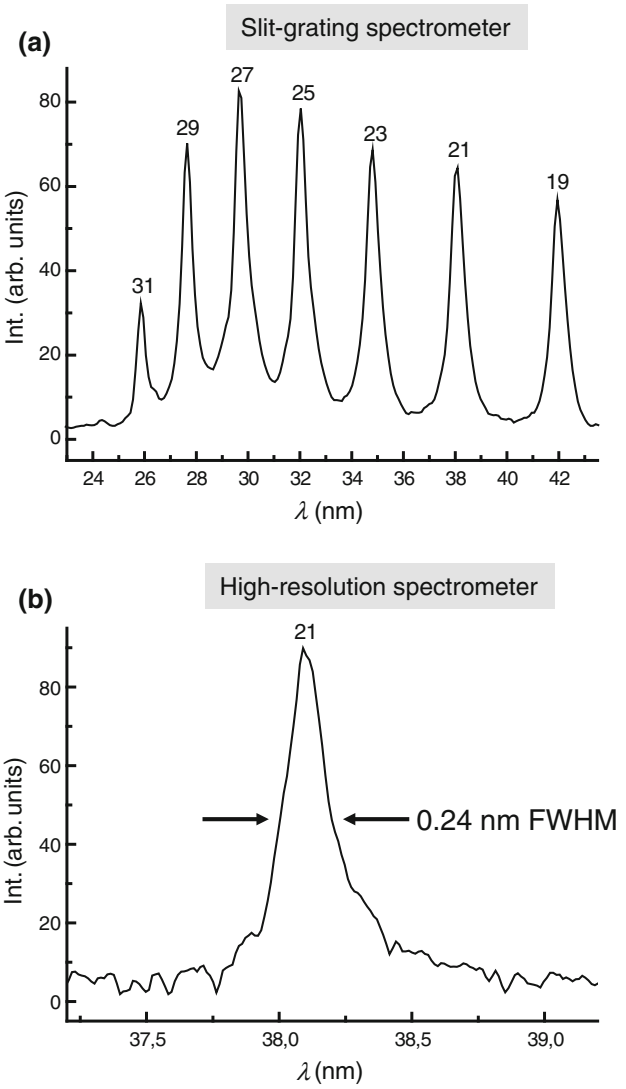

Fig. 3 HHG spectrum of the 800 nm laser in a pulsed argon gas target: **a** Slit-grating spectrum (harmonic orders are marked). The cutoff is found at the 31st harmonic. **b** High-resolution spectrum of the 21st harmonic behind the sFLASH undulators

mirrors (Fig. 1), which were manufactured to $\lambda/20$ precision (referring to the standard 633 nm wavelength). The source widths can be approximated with geometrical optics by multiplying with 2.28 to: $w_{0,21,x,\mathrm{source}} = (162 \pm 23)$ μm and $w_{0,21,y,\mathrm{source}} = (68 \pm 18)$ μm.

Additionally, the far-field branch can be used to monitor the pointing stability of the source over time. Therefore, the EUV-CCD is positioned between the two astigmatic foci at $z = 280$ mm, and the center-of-mass in x and y direction is evaluated. The average width at $z = 280$ mm is $\overline{w_{21}} = 82\,\mu$m. The position stability over 440 single shots in x and y directions is 6–9 % and 16–17 % (rms) of $\overline{w_{21}}$, respectively, depending on the daily laser stability. Thus, the center-of-mass fluctuations are smaller than the average width of the 21st harmonic.

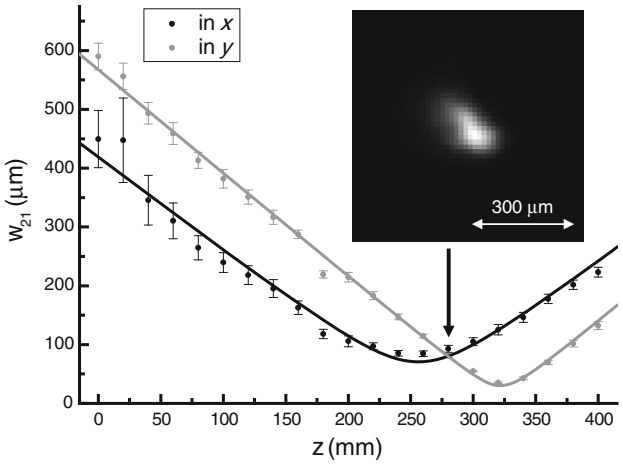

Fig. 4 Diagnostic-focus scan (2.28:1 demagnified image with $f_{21} = 1.5$ m) of the 21st harmonic: An astigmatism of 66 mm is observed. *Inset* picture of 21st harmonic focus at the indicated position

The focussing mirror is replaced by a plane one for the characterization of the near-field beam properties. The widths of the beam profile in x and y directions are 5.2 and 3.1 mm, respectively. At a distance of 7.05 m from the source, this corresponds to a half-angle of 0.74 and 0.44 mrad, respectively. It is well below the 1 mrad limit requested for the long injection beamline of sFLASH.

Seeding requires a reliable knowledge about the seed pulse energy. For the single-shot pulse-energy measurement of the 21st harmonic, the calibrated EUV-CCD and diodes were used. For both measurements, thin Al filters are necessary for blocking the NIR laser beam. Consequently, the energy measurement critically depends on a proper estimate of their transmission at 38.1 nm. The Al foils carry Al_2O_3 oxide layers on both sides, which influence the total transmission T to a large extent. Two filter combinations are used to deduce the transmission of 200 nm Al (T_{200}) and of a single oxide layer (T_{ox}) illustrated in Fig. 5. The energy of the 21st harmonic is measured in the far-field branch behind two multilayer mirrors for wavelength selectivity. The different Al filter configurations can be selected with a linear mover under constant HHG source conditions. In case (a), the 21st harmonic energy in front of (E_0) and behind (E_1) the 200 nm Al filter with two oxide layers is:

$$E_1 = E_0 \cdot T_{200} \cdot T_{ox}^2 \tag{4}$$

If we switch to the 400 nm Al filter and assume that both filters have the same oxide thickness and that the HHG source energy remains constant, the energy behind the 400 nm filter E_2 is given by:

$$E_2 = E_0 \cdot T_{200}^2 \cdot T_{ox}^2 \tag{5}$$

The ratio between the total background-corrected signals E_1 and E_2 was found to be:

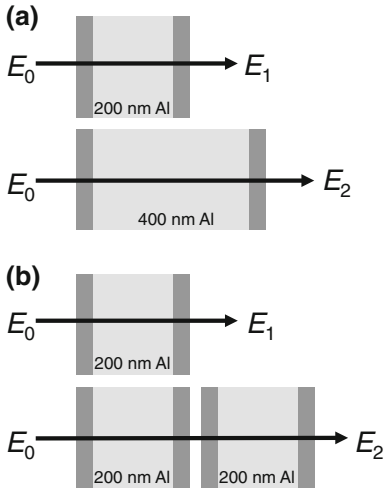

Fig. 5 Transmission determination of the 21st harmonic (38.1 nm) through different Al filters: **a** From the filter configurations, one can deduce the transmission of 200 nm Al (without oxide). **b** This configuration yields the transmission of a single Al_2O_3 oxide layer (*dark gray*)

$$E_2/E_1 = T_{200} = 0.52 \pm 0.11 \tag{6}$$

This measurement was repeated several times in order to exclude an unstable source. Additionally, all filters were delivered and mounted on the same day and were exposed to the same aging in air. The nominal transmission [36] at 38.1 nm of $T_{200,\mathrm{CXRO}} = 0.61$ is close to our measured value.

Under the same assumptions as above, the equations for case (b) are:

$$E_1 = E_0 \cdot T_{200} \cdot T_{ox}^2 \tag{7}$$

and

$$E_2 = E_0 \cdot T_{200}^2 \cdot T_{ox}^4 \tag{8}$$

Again, E_1 and E_2 can be measured and together with the known T_{200} from above yield the transmission of the single oxide layer:

$$E_2/E_1 = T_{200} \cdot T_{ox}^2 \Rightarrow T_{ox} = 0.82 \pm 0.10 \tag{9}$$

Thus, the full transmission of a single 200 nm Al filter at 38.1 nm is:

$$T = T_{200} \cdot T_{ox}^2 = 0.35 \pm 0.11 \tag{10}$$

An Al_2O_3 transmission of 0.82 ± 0.10 corresponds to an oxide layer thickness of only $2.7^{+1.7}_{-1.5}$ nm (calculated with [36]). Similar oxide thicknesses are reported from surface-science measurements: In [37], the aging effects of Al oxides in air were studied and an oxide layer of 1.8 nm shortly after manufacturing was found. Studies using

electron spectroscopy report a native oxide thickness of 4.2 nm [38]. The oxidation of Al clusters was simulated with a molecular dynamics approach [39]. They calculate an oxide thickness of 3–4 nm.

An oxide thickness of 2.7 nm is in good correspondence to surface-science literature but is smaller than assumed in some HHG-related publications. If the transmission of the filters is not measured and a thicker oxide layer is assumed, the generated EUV energy may easily be overestimated, especially if a set of filters are used to safely block the fundamental NIR light.

The Al filters characterized at 38.1 nm were combined with the EUV-CCD in the far-field branch, the diode in the injection beamline, and, additionally, a diode in front of the first sFLASH undulator for measuring the seed pulse energy at 38.1 nm. The pulse energy in the source can then be inferred by taking into account the transmission of the corresponding set of mirrors (see Fig. 1). The most direct detection is performed at diode D1 with no mirror reflections involved, but since no narrow spectral filter is used, the signal integrates over harmonic orders between 11 and 31. Taking into account the spectral variation within this band-pass and the quantum efficiencies and transmission coefficient of each harmonic, the 21st harmonic pulse energy in the source can be deduced [17]. Figure 6 displays 430 single-shot 21st harmonic pulse energies after HHG optimization. An average of 19.5 nJ with 5 % rms fluctuations is found. With a NIR pulse energy of 15 mJ at the target (iris slightly closed for optimization), this leads to a conversion efficiency into the 21st harmonic of 1.3×10^{-6}. This is close to the theoretical limit of about 2×10^{-6} calculated for 800 nm, 2 mJ, tight focus, 35 fs, with 2.3×10^{15} W/cm^2 [40].

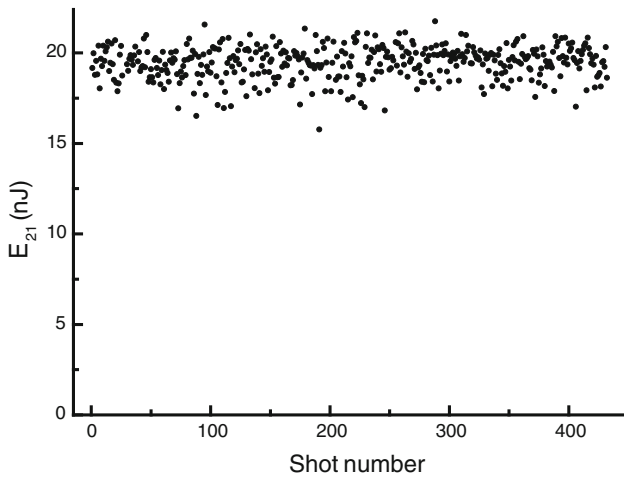

Fig. 6 Single-shot pulse energy of the 21st harmonic at the source measured with the EUV-CCD (430 shots with average 19.5 nJ and 5 % rms fluctuations)

A properly optimized and thermalized laser holds this performance constant over several hours or even days of operation.

For seeding, the Al filters (D1) are removed; therefore, only the beamline transmission from the source to the first sFLASH undulator of 5 % is taken into account. Thus, almost 1 nJ is expected at the undulator. This value is reproduced with a diode, which is located in front of the first undulator (D3). Longitudinal and transversal overlap between EUV seed and electron bunch results in a coupling efficiency of about 25 %; thus, around 250 pJ is effectively contributing to the seeding process, which is higher than the 20 pJ SASE noise of the undulator.

Note that looser focussing of the NIR can extend the Rayleigh length and, therefore, the interaction length between laser pulse and target medium. For example, pulse energies >100 nJ can be reached by focussing with $f_{\mathrm{NIR}} = 4$–5 m [41, 42]. As explained in the introduction, fluence in the undulator is for seeding the important

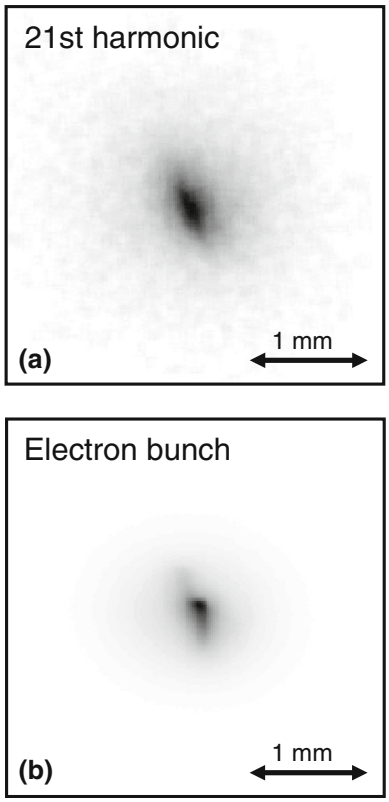

Fig. 7 Image of **a** 21st harmonic beam profile and **b** electron bunch on a Ce:YAG screen 1 m in front of the first seeding undulator module of sFLASH. Note that the Ce:YAG screen is in front of the actual HHG focus

parameter not only energy. Enhancing of the HHG pulse energy due to looser focussing is futile, because the further gain in energy cannot be coupled into the electron bunch. Therefore, at sFLASH the optimal HHG source width is given by the electron bunch, and only the efficiency was optimized.

3.3 HHG refocussing into the first sFLASH undulator module

From the diagnostic-focus scans shown above, we could deduce an average width of $\overline{w_{21}} = 82\ \mu$m. This corresponds to an expected average source width of 187 µm (2.28:1 image) and an expected width at the first undulator of 224 µm (1:1.2 image). The beam profile of the 21st harmonic can be directly measured behind a 200 nm Al filter on the Ce:YAG screen unit in D3, which is inserted 1 m in front of the first undulator. As depicted in Fig. 7a, widths of $w_{21,x,\mathrm{und}} = 552$ µm and $w_{21,y,\mathrm{und}} = 562$ µm are found being close to the widths of the electron bunch $w_{e,x,\mathrm{und}} = 332$ µm and $w_{e,y,\mathrm{und}} = 358$ µm, which is imaged on the same Ce:YAG screen shown in Fig. 7b. Although a detailed focus scan is not possible, a set of similar screens in the beam path allow us to establish a model for seed beam propagation. This analysis suggests a position of the focus 15.3 m behind M2, i.e., a location well within the first undulator [25]. Correspondingly, the widths are expected to be further reduced with respect to the values obtained at the Ce:YAG screen of Fig. 7a.

4 Conclusion

We presented in this article the HHG source which directly seeds sFLASH at 38.1 nm. We showed the experimental setup and discussed the diagnostics for tailoring and analyzing the seeding EUV radiation including spectrum, focus scan, and energy measurement. Limited available space and radiation protection measures have put serious constraints on the layout of the high-harmonic source and the EUV transport beamline. Still, an efficient HHG source could be realized that delivers seed pulses with remarkable stability. Since precise knowledge about absolute photon numbers is of utmost importance for a successful seeding, large effort was put in energy metrology. Careful measurements reveal the transmission of the Al filters and the oxide layer thickness. Thereby, pulse energies on the 20 nJ level in the relevant harmonic order of 38.1 nm in the HHG source could be deduced. The EUV wavelength regime prohibits the use of simple metallic mirrors near normal incidence, so that even after a careful optimization of the beamline, a total loss of 95 % had to be accepted. The remaining energy in the undulator together with the spatial overlap of electron bunch and seed pulse results in a seed power level of a factor of 10 above the limit set by the SASE noise level. Consequently, direct seeding at 38.1 nm could recently be demonstrated using this seed source [23, 24].

Acknowledgments The authors thank DESY and the FLASH team for the opportunity to perform the seeding experiment. All co-workers in the sFLASH team are gratefully acknowledged for helpful discussions and suggestions. The mechanical workshops of the University of Hamburg and DESY, as well as Oliver Becker, are acknowledged for technical support. We are financially supported by the Federal Ministry of Education and Research of Germany within FSP-301 under FKZ 05K10GU1, the German Research Foundation within GrK 1355, and SFB 925.

References

1. E.L. Saldin, E.A. Schneidmiller, M.V. Yurkow, *The Physics of Free Electron Lasers* (Springer, Berlin, 2000)
2. V. Ayvazyan et al., Eur. Phys. J. D **37**, 297 (2006)
3. W. Ackermann et al., Nat. Photonics **1**, 336 (2007)
4. K. Tiedtke et al., New J. Phys. **11**, 023029 (2009)
5. M. Richter et al., Appl. Phys. Lett. **83**, 2970 (2003)
6. U. Frühling et al., Nat. Photonics **3**, 523 (2009)
7. Th. Maltezopoulos et al., New J. Phys. **10**, 033026 (2008)
8. M. Krikunova et al., New J. Phys. **11**, 123019 (2009)
9. M. Krikunova et al., J. Chem. Phys. **134**, 024313 (2011)
10. M. Harmand et al., Nat. Photonics **7**, 215 (2013)
11. M. Drescher et al., J. Phys. B At. Mol. Opt. Phys. **43**, 194010 (2010)
12. V. Miltchev et al., in *Proceedings of FEL 2009 in Liverpool*, WEPC05
13. J. Bödewadt et al., in *Proceedings of FEL 2010 in Malmö*, WEOAI2
14. V. Miltchev et al., in *Proceedings of IPAC 2011 in San Sebastian*, TUZA02
15. C. Winterfeldt et al., Rev. Mod. Phys. **80**, 117 (2008)
16. F. Krausz et al., Rev. Mod. Phys. **81**, 163 (2009)
17. X. He et al., Phys. Rev. A **79**, 063829 (2009)
18. G. Lambert et al., New J. Phys. **11**, 083033 (2009)
19. C. Erny et al., New J. Phys. **13**, 073035 (2011)
20. G. Lambert et al., Nat. Phys. **4**, 296 (2008)
21. T. Togashi et al., Opt. Express **19**, 317 (2011)
22. M. Labat et al., Phys. Rev. Lett. **107**, 224801 (2011)
23. C. Lechner et al., in *Proceedings of FEL 2012 in Nara*, TUOAI01
24. S. Ackermann et al., Phys. Rev. Lett. (2013)
25. J. Bödewadt, PhD Thesis (2011), http://www.physnet.uni-hamburg.de/services/fachinfo/disslist2011.php
26. S. Ackermann et al., in *Proceedings of FEL 2011 in Shanghai*, TUPA31
27. P. Schmueser, M. Dohlus, J. Rossbach, *Ultraviolet and Soft X-Ray Free-Electron Lasers* (Springer, Berlin, 2009)
28. Z. Huang, Nucl. Instrum. Methods Phys. Res. A **475**, 59 (2001)
29. M. Felber et al., in *Proceedings of FEL 2010 in Malmö*, THOA3
30. M. Mittenzwey, PhD Thesis (2011), http://www.physnet.uni-hamburg.de/services/fachinfo/disslist2011.php
31. T. Wilhein et al., Rev. Sci. Instrum. **70**, 1694 (1999)
32. L. Miaja-Avila et al., Phys. Rev. Lett. **97**, 113604 (2006)
33. T. Sekikawa et al., Phys. Rev. Lett. **91**, 103902 (2003)
34. N. Reng, B. Eppich, Opt. Quantum Electron. **24**, 973 (1992)
35. T.F. Johnston, Appl. Opt. **37**, 4840 (1998)
36. The Center for X-Ray Optics, http://www.cxro.lbl.gov

37. F.R. Powell et al., Opt. Eng. **29**, 614 (1990)
38. B.R. Strohmeier, Surf. Interface Anal. **15**, 51 (1990)
39. T. Campbell et al., Phys. Rev. Lett. **82**, 4866 (1999)
40. E.L. Falcão-Filho et al., Appl. Phys. Lett. **97**, 061107 (2010)
41. E. Takahashi et al., Opt. Lett. **27**, 1920 (2002)
42. H. Mashiko et al., Opt. Lett. **29**, 1927 (2004)